

# COMPARATIVE STUDY OF ANN-BASED AND CONVENTIONAL METHODS FOR POWER QUALITY IMPROVEMENT IN MICROGRIDS

Chetna Kumari Jain, Raunak Jangid, Manisha Sisodiya, Vikas Garg

E-Mail Id: raunakee.85@gmail.com, jainchetna953@gmail.com

Department of Electrical Engineering, Geetanjali Institute of Technical Studies, Udaipur, Rajasthan, India

**Abstract-** This paper presents a novel approach to addressing power quality issues that arise from the unpredictable nature of renewable energy sources such as solar and wind. In standalone hybrid systems combining solar photovoltaic (PV) arrays and wind turbine generators (WTGs), fluctuations in power output can result in voltage instability, frequency variation, and harmonic distortion, all of which affect the reliability of power delivery. Conventional power conditioning methods, including passive filters and voltage regulators, often fail to respond effectively to rapid and irregular changes in energy input. To overcome these limitations, this study proposes the integration of a DVR managed by an Artificial Neural Network (ANN). The ANN is trained using historical performance data to identify patterns associated with various power disturbances. Once deployed, it monitors the system in real time, detecting anomalies and activating the DVR to inject appropriate compensating voltages. This dynamic correction restores load voltage to acceptable limits, ensuring system stability. Simulation tests conducted on a hybrid PV-wind model validate the effectiveness of the proposed system, showing significant improvements in voltage regulation and overall power quality. This method provides a smart, adaptive solution for enhancing the performance of standalone renewable energy systems.

**Keywords:** PV, WECS, Battery, ANN, ESS, standalone hybrid system.

## 1. INTRODUCTION

The escalating global energy demand, coupled with the depletion of conventional fossil fuel reserves, has intensified the pursuit of sustainable and environmentally friendly energy alternatives. Renewable energy sources (RES), notably solar and wind, have emerged as pivotal in this transition due to their abundance and minimal environmental impact. India, recognizing the imperative for clean energy, has embarked on one of the world's most ambitious renewable energy expansion programs. As of January 2025, India's installed renewable energy capacity has reached approximately 217.62 GW, marking a significant stride towards the national target of 500 GW of non-fossil fuel-based energy capacity by 2030. This growth is underscored by record additions in 2024, including 24.5 GW of solar capacity and 3.4 GW of wind capacity. Solar energy now constitutes nearly 47% of the total renewable capacity, reflecting its central role in India's energy strategy.

Despite these advancements, the intermittent and unpredictable nature of solar and wind energy poses challenges to power quality and reliability. Fluctuations in generation can lead to voltage instability, frequency deviations, and harmonic distortions, particularly in standalone systems. To mitigate these issues, the integration of energy storage systems, such as batteries and supercapacitors, is essential. These storage solutions not only buffer the variability of RES but also ensure a consistent energy supply to meet demand.

This research focuses on the design, dynamic modeling, and control strategies of standalone hybrid solar-wind energy systems. By incorporating advanced artificial intelligence (AI) techniques, specifically artificial neural networks (ANN), the study aims to enhance energy management and system stability. The proposed AI-based control system is trained on historical data to predict and respond to power quality disturbances in real-time, thereby optimizing the performance of hybrid RES installations. Through simulation and analysis, the study evaluates the efficacy of the ANN-controlled system in maintaining voltage and frequency stability under varying operational conditions.

## 2. DESCRIPTION OF PROPOSED CONFIGURATION AND MODELING OF THE HRES

The proposed microgrid configuration integrates a hybrid solar photovoltaic (PV) and wind energy system with a Hybrid Energy Storage System (HESS) to supply power to an off-grid community. The PV array is connected through a DC-DC boost converter, while the Wind Energy Conversion System (WECS) employs an Optimal Torque (OT) based Maximum Power Point Tracking (MPPT) technique via its own boost converter. Both sources feed into a common DC link maintained at 650 V.

The HESS comprises battery banks and supercapacitors, interfaced through a bidirectional DC-DC converter managed by an Artificial Neural Network (ANN) controller. This controller dynamically regulates charging and discharging cycles based on real-time load demands and generation availability. When generation exceeds

DOI Number: <https://doi.org/10.30780/IJTRS.V10.I06.007>

pg. 47

[www.ijtrs.com](http://www.ijtrs.com), [www.ijtrs.org](http://www.ijtrs.org)

Paper Id: IJTRS-V10-I05-007

Volume X Issue VI, June 2025

@2017, IJTRS All Right Reserved

consumption, the battery charges first; if its charging current surpasses a predefined threshold, the supercapacitor engages to absorb excess energy. Conversely, during high load demand, the battery discharges, and if its current exceeds the set limit, the supercapacitor supplements the supply to maintain system stability.

To cater to AC loads, a Voltage Source Converter (VSC) inverter, governed by a fuzzy logic controller, converts DC to AC power. At the Point of Common Coupling (PCC), a Dynamic Voltage Restorer (DVR) is deployed to mitigate voltage sags and swells, enhancing power quality. The DVR operates by injecting compensatory voltages through a voltage source inverter connected via an injecting transformer, addressing discrepancies between supply and load feeders (F1 and F2). An LC filter is incorporated to suppress harmonics, ensuring the delivery of clean power.

This integrated system design aims to provide a reliable and efficient power supply, particularly in remote areas, by effectively managing the intermittency of renewable energy sources and maintaining power quality standards.

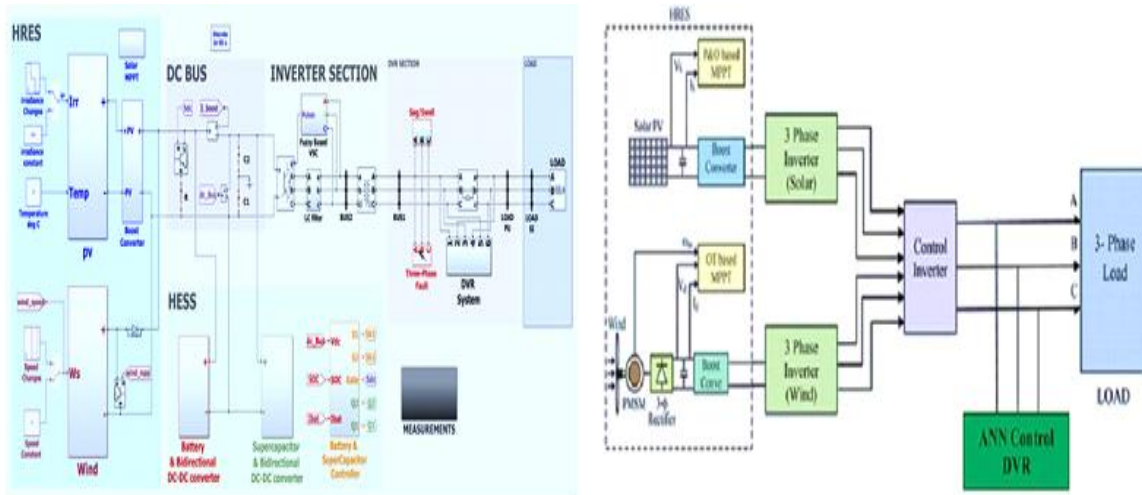


Fig. 2.1 Block Diagram of Dynamic Model for Hybrid Solar PV Wind Microgrid

### 3. PV SYSTEM MODELING

The equivalent circuit of a PV cell is shown in Fig. 3.1. The current source  $I_{ph}$  represents the cell photocurrent.  $R_{sh}$  and  $R_s$  are the intrinsic shunt and series resistances of the cell, respectively. Usually the value of  $R_{sh}$  is very large and that of  $R_s$  is very small, hence they may be neglected to simplify the analysis. Practically, PV cells are grouped in larger units called PV modules and these modules are connected in series or parallel to create PV arrays which are used to generate electricity in PV generation systems. The equivalent circuit for PV array is shown in Fig. 3.2.

The voltage-current characteristic equation of a solar cell is provided:

$$\text{Module photo-current } I_{ph}: I_{ph} = [I_{SC} + K_1 (T - 298)] * I_r / 1000$$

Here:  $I_{ph}$ : photo-current (A),  $I_{SC}$ : short circuit current (A),  $K_1$ : short-circuit current of cell at 25 °C and 1000 W/m<sup>2</sup>, T: operating temperature (K),  $I_r$ : solar irradiation (W/m<sup>2</sup>).

$$\text{Module reverse saturation current } I_{rs}: I_{rs} = I_{sc} / [\exp (qV_{oc} / N_s kT) - 1]$$

Here: q: electron charge =  $1.6 \times 10^{-19}$ C,  $V_{oc}$ : open circuit voltage (V),  $N_s$ : number of cells connected in series, n: the ideality factor of the diode, k: Boltzmann's constant, =  $1.3805 \times 10^{-23}$  J/K.

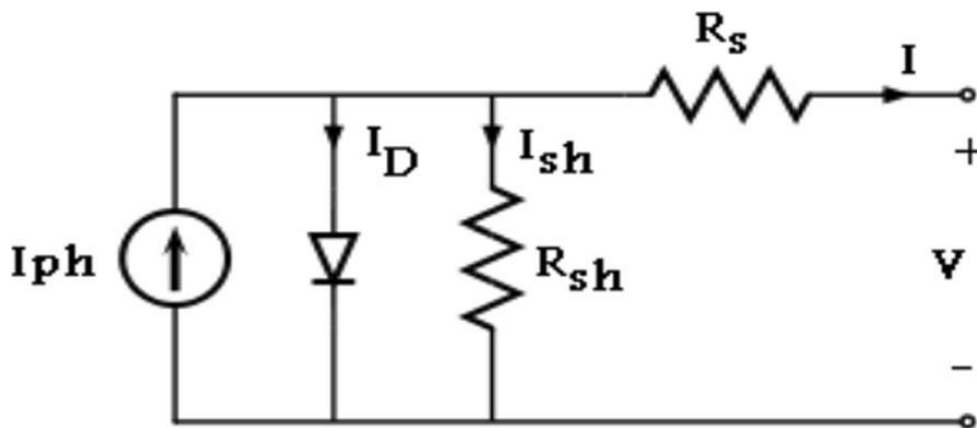
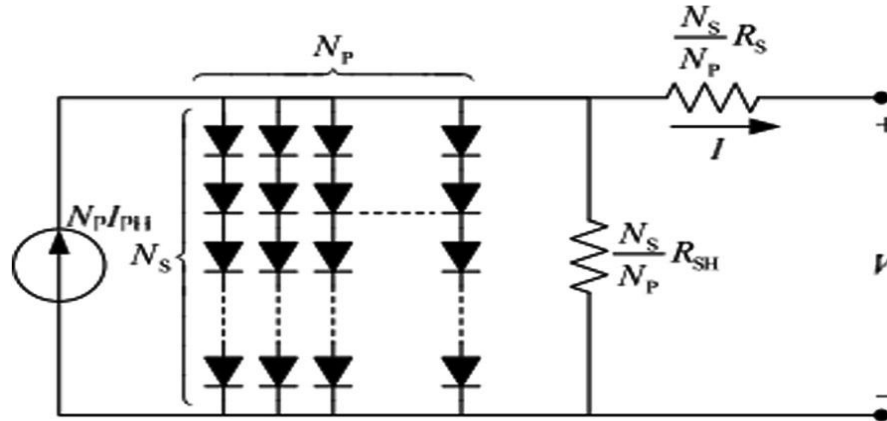


Fig. 3.1 PV cell equivalent Circuit


**Fig. 3.2 Equivalent Circuit of Solar Array**

The module saturation current  $I_0$  varies with the cell temperature, which is given by:

$$I_0 = I_{rs} \left[ \frac{T}{T_r} \right]^3 \exp \left[ \frac{q \times E_{g0}}{nk} \left( \frac{1}{T} - \frac{1}{T_r} \right) \right] \quad (1)$$

Here:  $T_r$ : nominal temperature = 298.15 K,  $E_{g0}$ : band gap energy of the semiconductor = 1.1 eV The current output of PV module is:

$$I = N_p \times I_{ph} - N_p \times I_0 \times \left[ \exp \left( \frac{V/N_s + I \times R_s/N_p}{n \times V_t} \right) - 1 \right] - I_{sh} \quad (2)$$

$$\text{With } V_t = \frac{k \times T}{q} \text{ and } I_{sh} = \frac{V \times N_p/N_s + I \times R_s}{R_{sh}}$$

Here:  $N_p$ : number of PV modules connected in parallel,  $R_s$ : series resistance ( $\Omega$ ),  $R_{sh}$ : shunt resistance ( $\Omega$ ),  $V_t$ : diode thermal voltage (V).

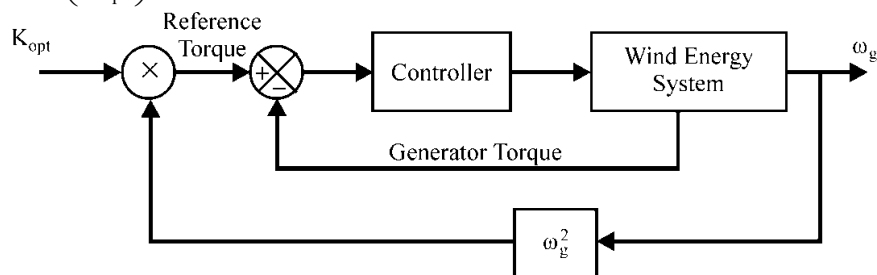
#### 4. WIND SYSTEM MODELING

The torque controller aims to enhance the efficiency of wind energy capture across a broad spectrum of wind speeds by ensuring the generated power remains at its optimum level. This is achieved through the block diagram depicted in Figure 4. Irrespective of the wind velocity, the Maximum Power Point Tracking (MPPT) tool imposes a torque reference capable of extracting the maximum available power. The curve  $T_{opt}$  is represented as:

$$T_{opt} = K_{opt} * \omega_{opt}^2 \quad (3)$$

Where

$$K_{opt} = 0.5 * \rho A * \left( \frac{r_m}{\lambda_{opt}} \right)^3 * C_{P-max} \quad (4)$$


**Fig. 4.1 Optimal Torque Control MPPT Method**

The PMSG model is presented in figure. This dynamic model assumes no saturation, a sinusoidal back e.m.f. and negligible eddy current and hysteresis losses. It takes into account the iron losses and the dynamic equations for the PMSG currents are:

$$\frac{di_{md}}{dt} = \frac{1}{L_d} (v_d - R_{st} i_d + \omega L_q i_{mq}), \quad (5)$$

$$\frac{di_{mq}}{dt} = \frac{1}{L_d} (v_q - R_{st} i_q + \omega L_q i_{md} - \omega \Psi_{PM}), \quad (6)$$

$$i_d = \frac{1}{R_c} (L_d \frac{di_{md}}{dt} - \omega L_q i_{mq} + R_c i_{md}), \quad (7)$$

$$i_q = \frac{1}{R_c} (L_q \frac{di_{mq}}{dt} + \omega L_d i_{md} + \omega \psi_{PM} + R_c i_{mq}), \quad (8)$$

$$i_{cd} = i_d - i_{md}, \quad (9)$$

$$i_{cq} = i_q - i_{mq}, \quad (10)$$

where  $i_d, i_q$  are the  $d_q$  axes currents,  $V_d, V_q$  are the  $d_q$  axes voltages,  $i'_{cd}, i_{cq}$  are the  $d_q$  axes iron losses currents,  $i_{md}, i_{mq}$  are the  $d_q$  axes magnetizing currents,  $L_d, L_q$  are the  $d_q$  axes inductances,  $\psi_{PM}$  is the mutual flux due to magnets,  $\omega$  is the fundamental frequency of the stator currents,  $R_c$  is the iron losses resistance and  $R_{st}$  is the stator resistance.

$$\text{The electromagnetic torque equation of the PMSG is: } T_e = \frac{2}{3} p [\psi_{PM} i_{mq} + (L_d - L_q) i_{md} i_{mq}] \quad (11)$$

where  $p$  is the number of pole pairs

## 5. MODELING OF BATTERIES

The Battery block implements a basic dynamic model parameterized to be best common types of rechargeable batteries.

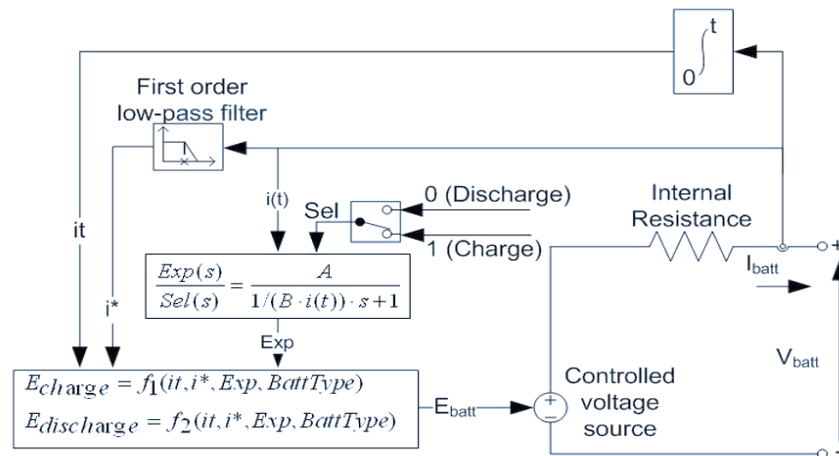


Fig. 5.1 Battery Equivalent Circuit

For the nickel-cadmium and nickel-metal-hydride battery types, the model uses these equations:

$$\text{Discharge Model (} i^* > 0 \text{)} \quad f_1(it, i^*, i, \text{Exp}) = E_0 - K \cdot \frac{Q}{Q - it} \cdot i^* - K \cdot \frac{Q}{Q - it} \cdot it + \text{Laplace}^{-1} \left( \frac{\text{Exp}(s)}{\text{Sel}(s)} \cdot 0 \right)$$

$$\text{Charge Model (} i^* < 0 \text{)} \quad f_2(it, i^*, i, \text{Exp}) = E_0 - K \cdot \frac{Q}{|it| + 0.1 \cdot Q} \cdot i^* - K \cdot \frac{Q}{Q - it} \cdot it + \text{Laplace}^{-1} \left( \frac{\text{Exp}(s)}{\text{Sel}(s)} \cdot \frac{1}{s} \right)$$

In the equations:

Here,  $E_{Batt}$  is nonlinear voltage, in V,  $E_0$  is constant voltage, in V,  $\text{Exp}(s)$  is exponential zone dynamics, in V,  $\text{Sel}(s)$  represents the battery mode,  $\text{Sel}(s) = 0$  during battery discharge,  $\text{Sel}(s) = 1$  during battery charging,  $K$  is polarization constant, in  $\text{Ah}^{-1}$ ,  $i^*$  is low frequency current dynamics, in A,  $i$  is battery current, in A.

$it$  is extracted capacity, in Ah.  $Q$  is maximum battery capacity, in Ah.,  $A$  is exponential voltage, in V.,  $B$  is exponential capacity, in  $\text{Ah}^{-1}$ .

## 6. SUPERCAPACITOR CONTROL STRATEGY

The role of supercapacitor Control Strategy is very important to make DC bus voltage constant and to remove the stress of the battery during pulsed load. The main focus of the proposed control scheme is on the supercapacitor reference ( $i_{sc,ref}$ ) current generation which depends on the battery reference ( $i_{B,ref}$ ) and battery error current ( $i_{error}$ ).

The current control of the supercapacitor is achieved by the control variable ( $D_{sc}$ ). In proposed control scheme supercapacitor quickly responds towards the sudden change occurs in DC bus voltage due to environmental change or load variation. Fig. 6 shows the control strategy for supercapacitor.

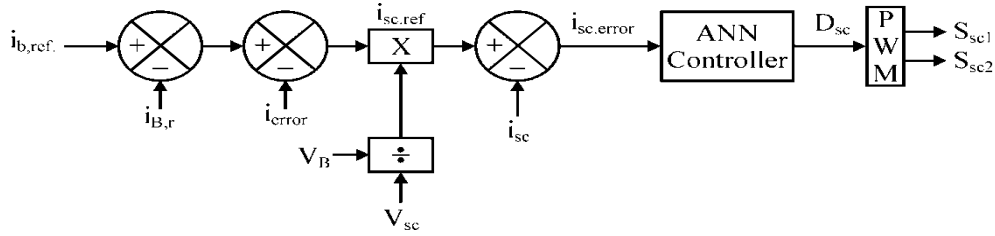


Fig. 6.1 Control Strategy for Supercapacitor

$$i_{sc,ref} = \left[ i_{B,ref} - i_{B,r} + i_{error} \right] \frac{V_B}{V_{sc}} \quad \dots 12$$

The supercapacitor reference current ( $i_{sc,ref}$ ) is obtained from battery reference current ( $i_{B,ref}$ ) and the gain of DC bus voltage estimator ( $G_{cv}$ ) is given by equation.

$$i_{sc,ref} = \left[ i_{B,ref} - \frac{2}{T} \int_{t_0}^{t_0+T} i_{B,ref} dt + i_B \right] \frac{V_B}{V_{sc}} \quad \dots 13$$

$$i_{sc,error} = \left[ i_{B,ref} - \frac{2}{T} \int_{t_0}^{t_0+T} i_{B,ref} dt + i_B \right] \frac{V_B}{V_{sc}} - i_{sc} \quad \dots 14$$

$$i_{sc} = i_{B,ref} \frac{V_B}{V_{sc}} - \frac{2V_B}{TV_{sc}} \int_{t_0}^{t_0+T} i_{B,ref} dt + \frac{V_B}{V_{sc}} i_B - i_{sc,error} \quad \dots 15$$

The supercapacitor state model during boost mode operation is given by:

$$v_{sc} = L_{sc} \frac{di_{sc}}{dt} + v_{dc} (1 - D_{sc}) \quad \dots 16$$

$$c_{sc} \frac{dv_{dc}}{dt} = i_{sc} (1 - D_{sc}) + \frac{v_{dc}}{R, L_{eq}} \quad \dots 17$$

$$i_{sc} = i_{sc} D_{sc} + c_{sc} \frac{dv_{dc}}{dt} - \frac{v_{dc}}{R, L_{eq}} \quad \dots 18$$

By solving 3.63 and 3.64, the control variable  $D_{sc}$  is obtained

$$D_{sc} = \frac{v_B}{i_{sc} v_{sc}} \left[ i_{B,ref} - \frac{2}{T} \int_{t_0}^{t_0+T} i_{B,ref} dt + i_B \right] - \frac{i_{sc,error}}{i_{sc}} - \frac{c_{sc} dv_{dc}}{i_{sc} dt} + \frac{v_{dc}}{i_{sc} R_{Leq}} \quad \dots 19$$

Where  $R_{Leq}$ , is the equivalent load resistance

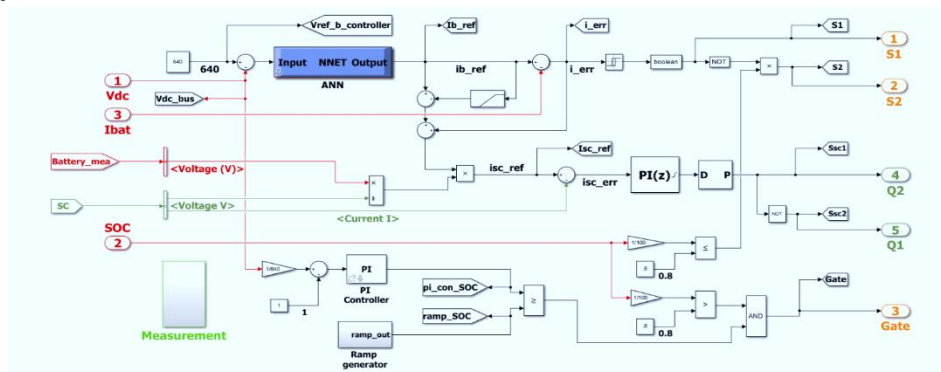


Fig. 6.2 Simulink Model of Novel Control Strategy

## 7. SIMULATION RESULTS AND DISCUSSION

In this case, the simulation results of an ANN-based DVR and a traditional DVR are compared using RMS Vph (load side & generating side). Both symmetrical and asymmetrical fault simulation findings are discussed below.

### Case-I: Comparison of Conventional and ANN-Based DVR Performance During Asymmetrical Faults

DOI Number: <https://doi.org/10.30780/IJTRS.V10.I06.007>

pg. 51

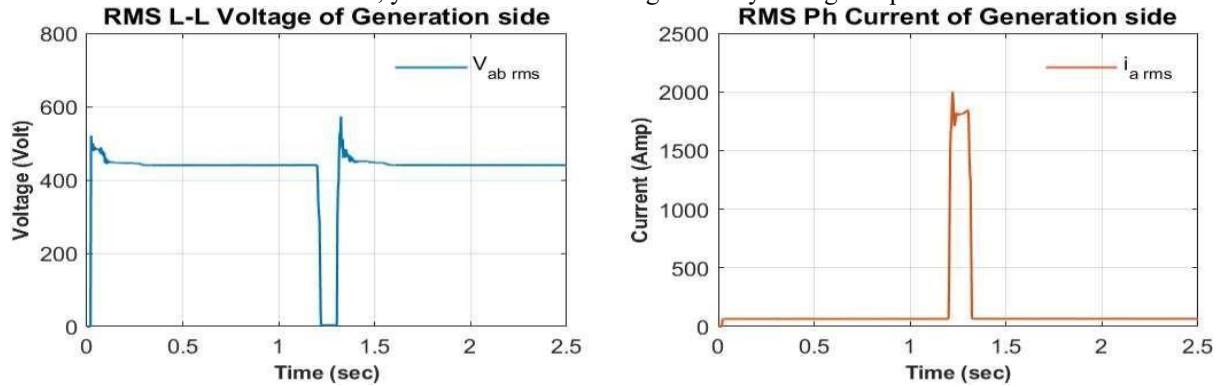
[www.ijtrs.com](http://www.ijtrs.com), [www.ijtrs.org](http://www.ijtrs.org)

Paper Id: IJTRS-V10-I05-007

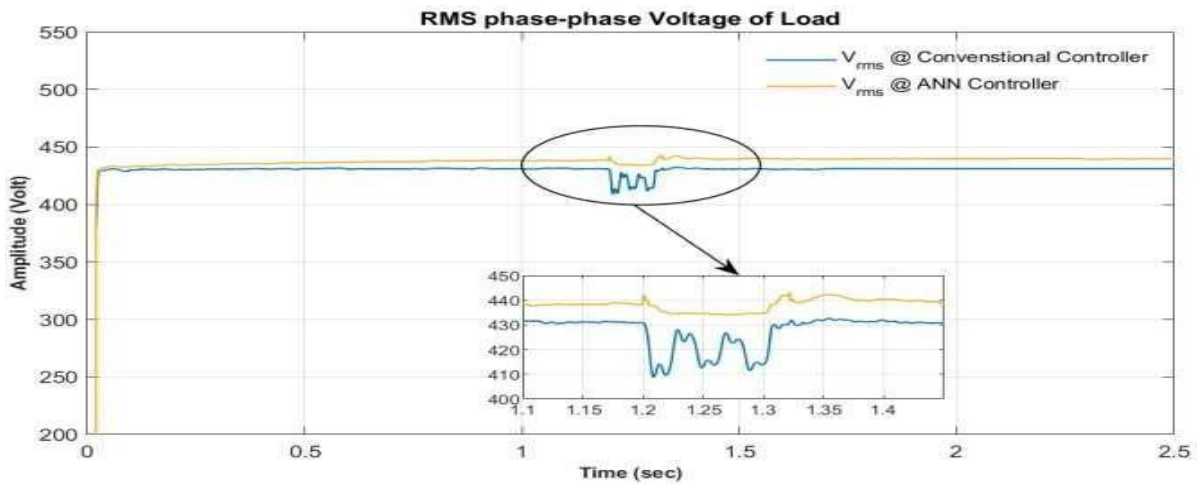
Volume X Issue VI, June 2025

@2017, IJTRS All Right Reserved

The following figures show the findings of the L-L fault simulation. At the generating side, the  $V_{rms}$  &  $I_{rms}$  waveforms are shown in Figure 7.1. The RMS  $V_{pp}$  (generating side). falls to zero during the L-L fault, which lasts from  $t = 1.2$  to  $t = 1.3$  seconds, yet the  $I_{rms}$  increases significantly during this period.



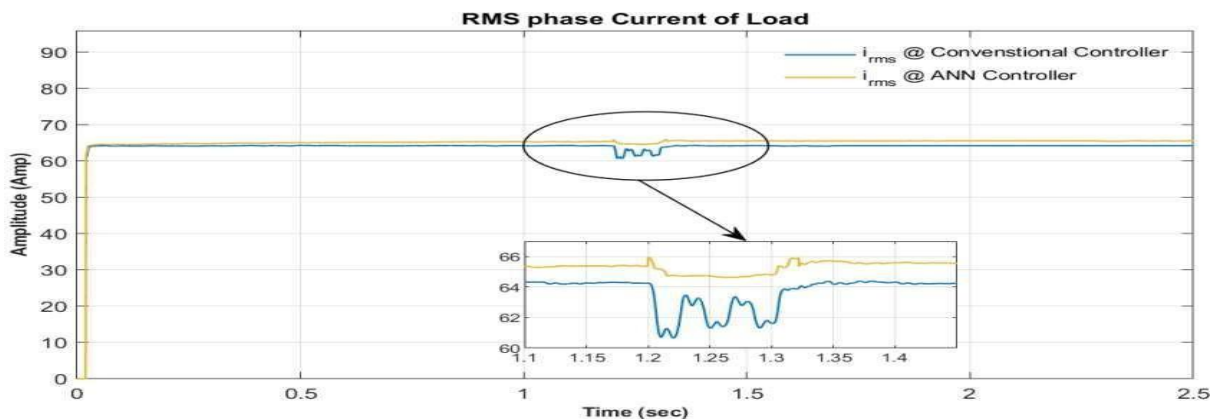
**Fig. 7.1 Comparison of Load RMS Voltage with Conventional DVR and ANN-Based DVR During L-L Fault**



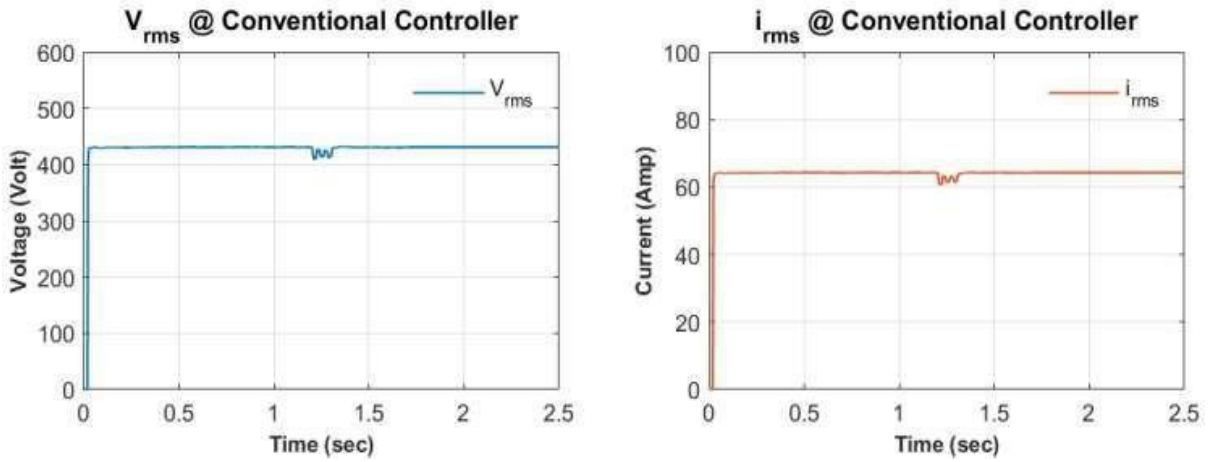
**Fig. 7.2 shows a comparison between an ANN-based DVR and a traditional DVR for the RMS  $V_{pp}$  on the Load Side**

It is clear that during the failure, the RMS  $V_{ph}$  on the load side is distorted from  $t = 1.2$  to  $1.3$  seconds when using a traditional DVR. Conversely, during the simulation, the ANN-tuned DVR keeps the RMS phase voltage at 440 V constant. In the figure's zoomed-in window, the RMS phase voltage at 430 V using the traditional DVR emphasizes this stability.

The RMS phase current on the load side is also significantly impacted when utilizing the traditional DVR, as Figure 7.3 illustrates. The RMS phase current, however, stays almost constant at 65.65 A with the ANN-tuned DVR. Additionally, this is seen in the figure's zoomed-in window, where the RMS phase current using the traditional DVR is 64.23 A.

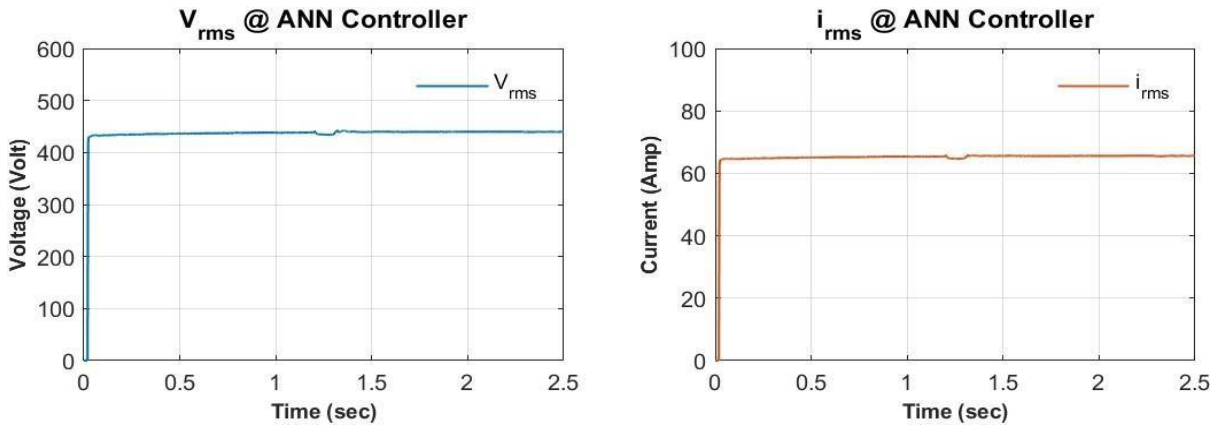


**Fig. 7.3 Load RMS Current Comparison: Conventional vs. ANN DVR During L-L Fault**



**Fig. 7.4 RMS Voltage and Current Waveforms with Conventional DVR During L-L Fault**

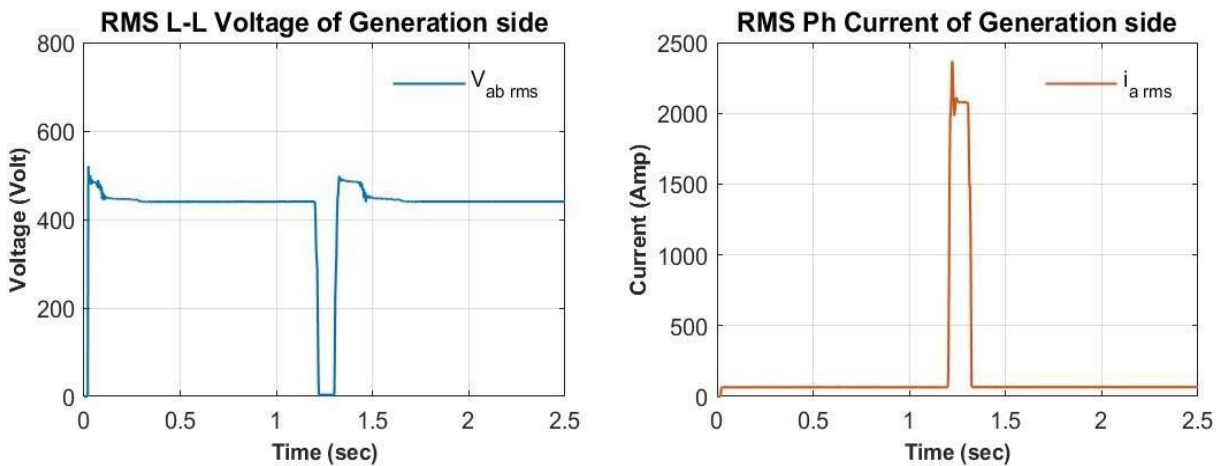
The RMS voltage and current are displayed with the traditional DVR in Figure 7.4 and with the ANN-based DVR in Figure 7.5. It is clear from these numbers that the ANN-based DVR performs better dynamically than the traditional DVR.



**Fig. 7.5 RMS Voltage and Current Waveforms with ANN-Based DVR During L-L Fault**

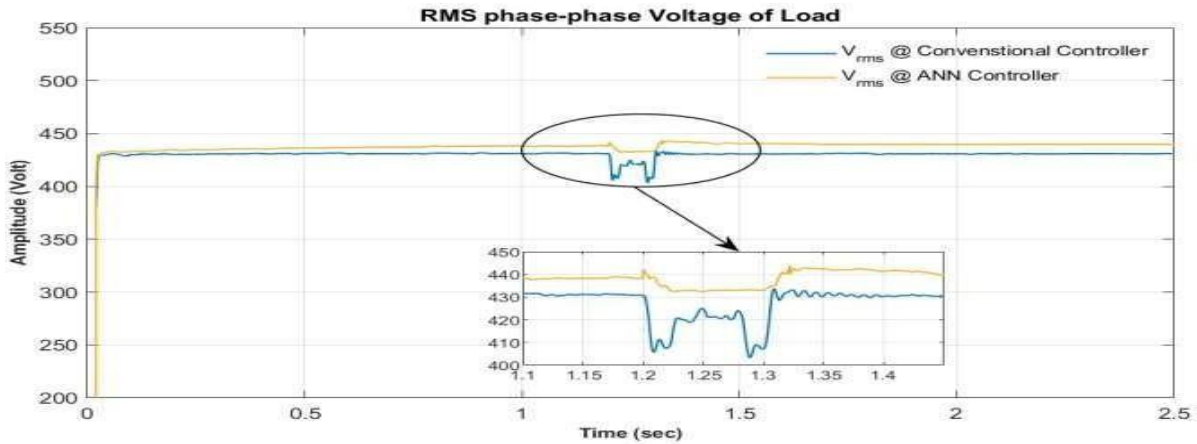
**Case-II: Comparison of Conventional and ANN-Based DVR Performance During Symmetrical Faults**

The following figures display the findings of the 3-phase L-G failure simulation. On the generating side, the RMS voltage and RMS current waveforms are shown in Figure 7.6. The generator side's RMS phase-to-phase voltage falls to zero during the fault, which lasts from  $t = 1.2$  to  $t = 1.3$  seconds, while the RMS phase current increases to a very high the quantity.



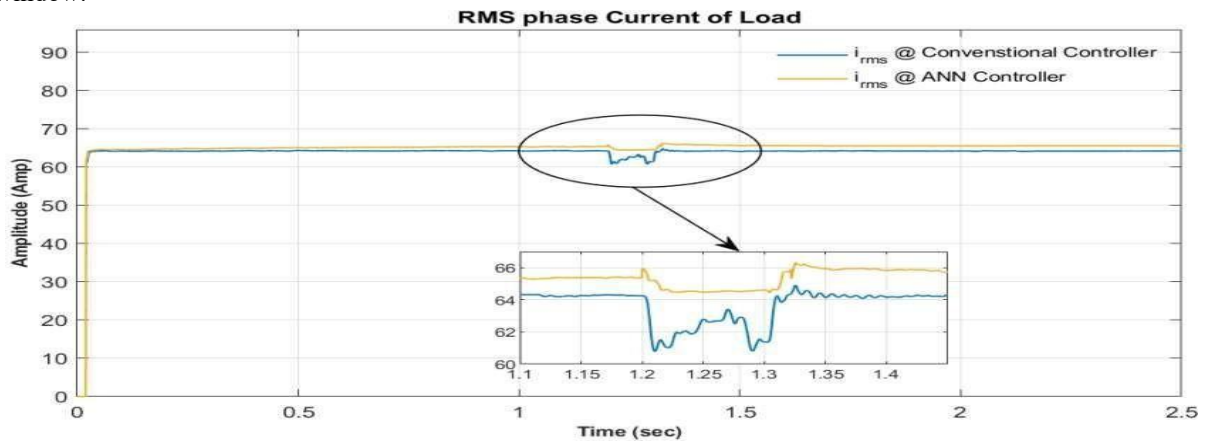
**Fig. 7.6 RMS  $V_{pp}$  and  $I_{ph}$  (Generation Side) During 3-Phase L-G Fault**

Figure 7.7 shows the difference between an ANN-based DVR and a traditional DVR in terms of the RMS  $V_{ph}$  (load side). It is clear that the RMS  $V_{ph}$  (load side) goes from  $t = 1.2$  to  $1.3$  seconds during the fault when using a traditional DVR. Conversely, during the simulation, the ANN-tuned DVR keeps the RMS phase voltage at 440 V constant. In the figure's zoomed-in window, which displays the RMS phase voltage at 430 V using the traditional DVR, this stability is further emphasized.

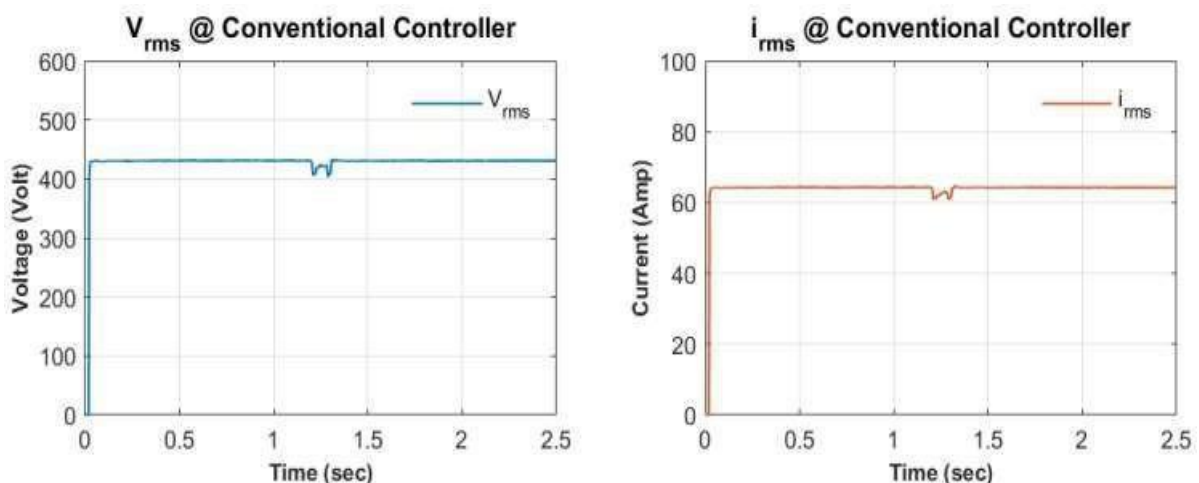


**Fig. 7.7 Comparison of Load RMS Voltage with Conventional vs. ANN DVR During 3-Phase L-G Fault**

The RMS phase current on the load side is also significantly impacted when utilizing the traditional DVR, as Figure 7.8 illustrates. On the other hand, the RMS phase current with the ANN-tuned DVR stays nearly constant at 65.65 A. With the traditional DVR, the RMS phase current is 64.23 A, as can be seen in the figure's zoomed-in window.

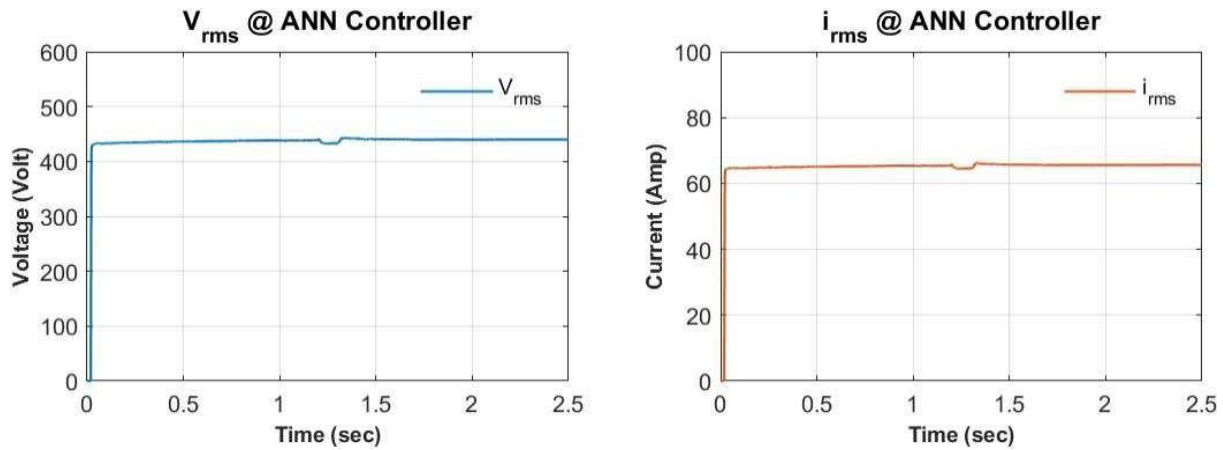


**Fig. 7.8 Comparison of Load RMS Current with Conventional vs. ANN DVR During 3-Phase L-G Fault**



**Fig. 7.9 RMS Voltage and Current Waveforms with Conventional DVR During 3-Phase L-G Fault**

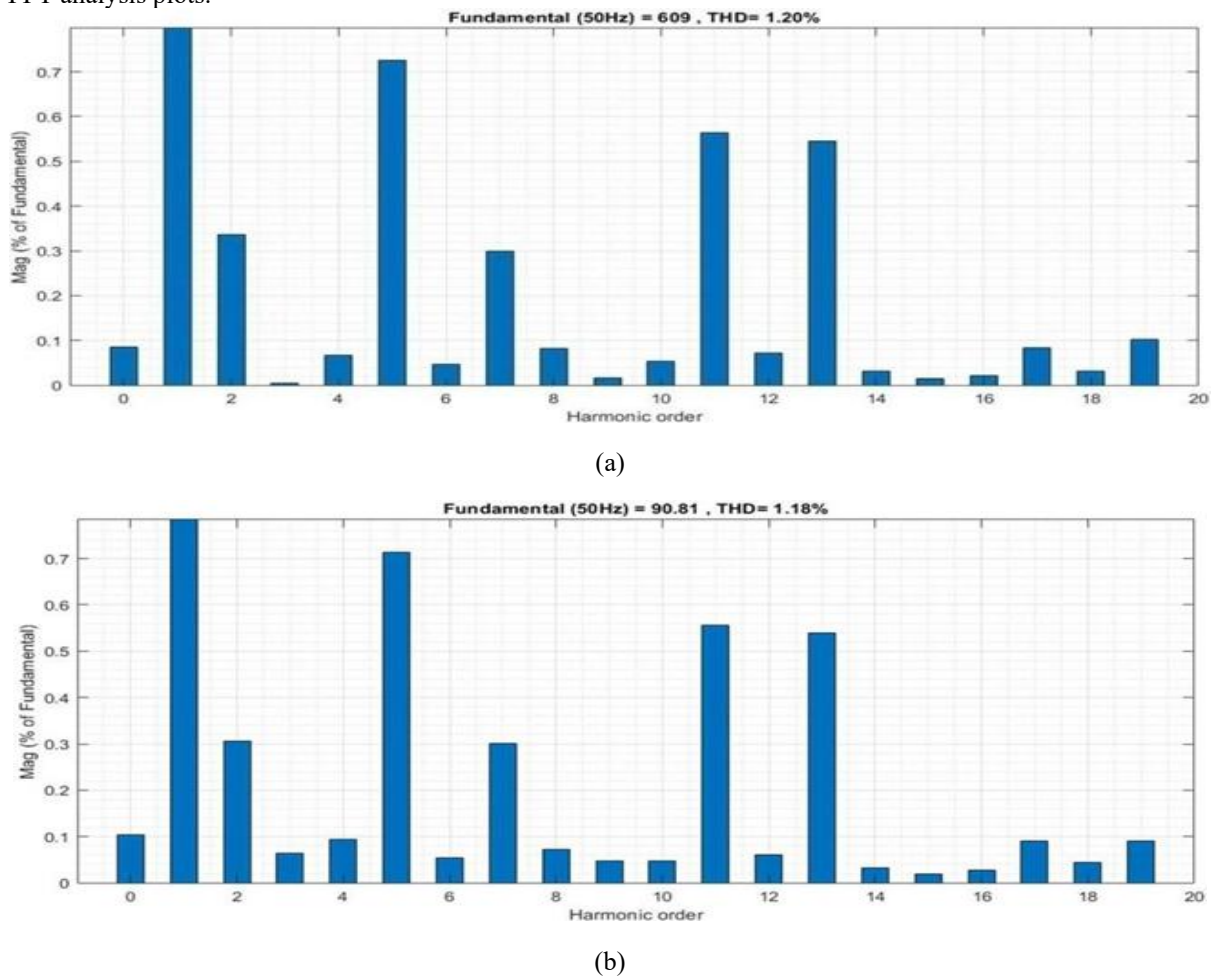
Figure 7.9 shows the RMS voltage and current with the ANN-based DVR, whereas Figure 7.10 shows same values with the traditional DVR. It's clear from the comparison that the ANN-based DVR performs better dynamically than conventional DVR.



**Fig. 7.10 RMS Voltage and Current Waveforms with ANN-Based DVR During 3-Phase L-G Fault**

**Case-III: FFT-Based Performance Analysis of ANN-Based DVR**

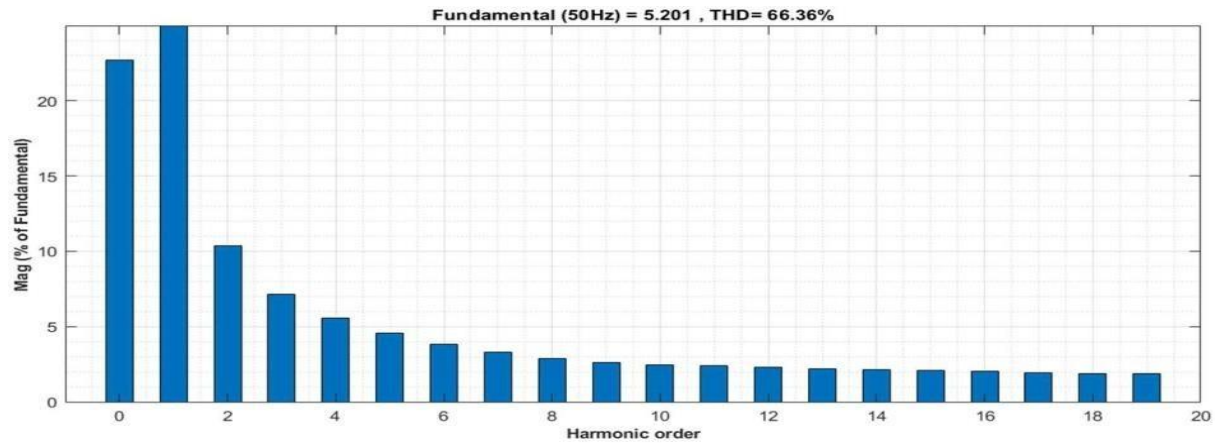
The following section discusses the performance analysis of the ANN-trained DVR, illustrating the results with FFT analysis plots.



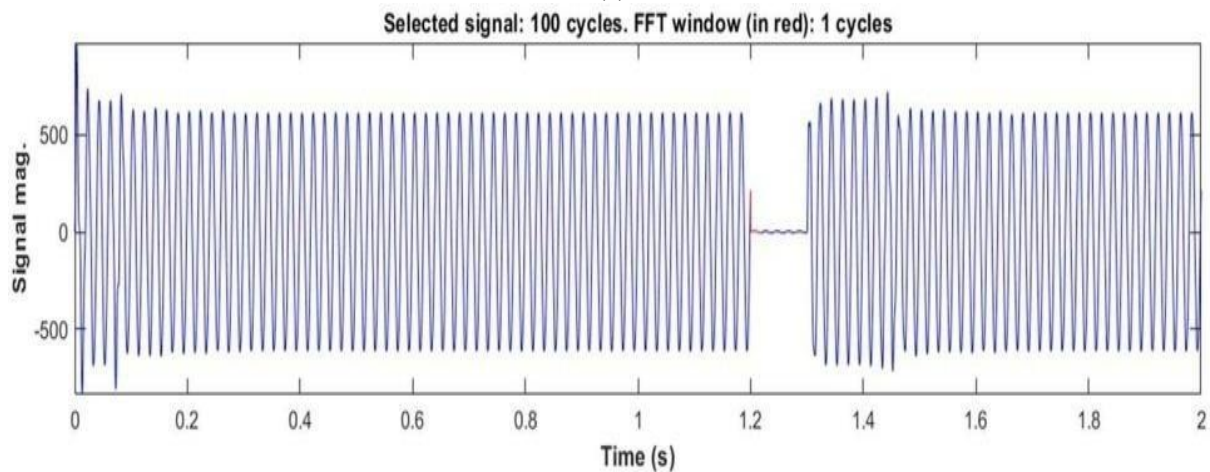
**Fig. 7.11 FFT Analysis of Load: (a) Vpp, (b) Iph Under Normal Conditions**

Figure 7.11 (a) and (b) show the FFT plots for the load's phase-to-phase voltage and phase-to-phase current, respectively. There is no system fault, and the total harmonic distortion (THD) for the phase-to-phase voltage is 1.20% at an amplitude of 609 V and for the phase current is 1.18% at an amplitude of 90.81 A. These load voltages

and current THD values fall within the acceptable ranges as defined by IEEE standards, which set a maximum of 5%.



(a)

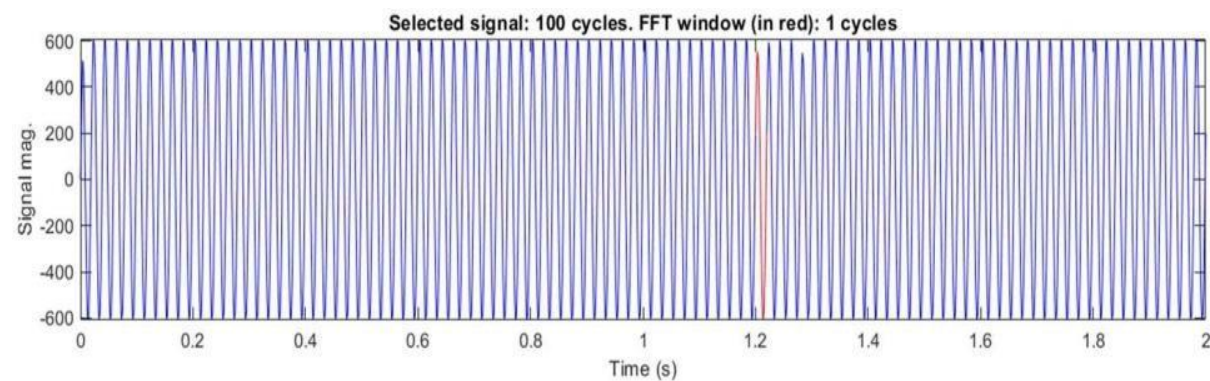


(b)

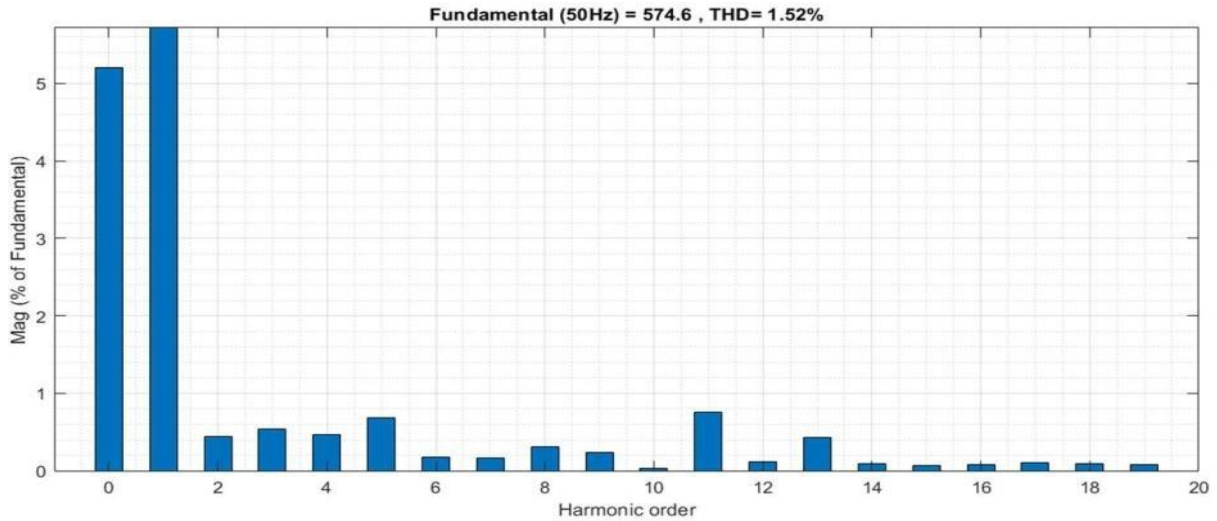
**Fig. 7.12 (a) Generation Side Phase-to-Phase Voltage Signal, (b) FFT Plot of Generation Side Phase-to-Phase Voltage Under Faulty Condition**

For the generating side and load side, the signal window and FFT plot for the phase- to-phase voltage are shown in Figure 7.11 (a) and (b), respectively. The FFT window has been obtained for a single signal cycle during a fault that occurs at time  $t=1.2$  seconds, as seen in Figures 7.11 (a) and (b).

As seen in Fig. 7.12 (b), the total harmonic distortion (THD) for the  $V_{pp}$  (generating side) during the fault is 66.36%, which is far higher than the IEEE standards' limit. However, as seen in Fig. 7.13 (b), the THD for the  $V_{pp}$  (load side) during the fault is 1.52% at an amplitude of 574.6 V, which is within IEEE standards' permissible bounds. Furthermore, the load side voltage has lower third and fifth harmonics than the generator side voltage.



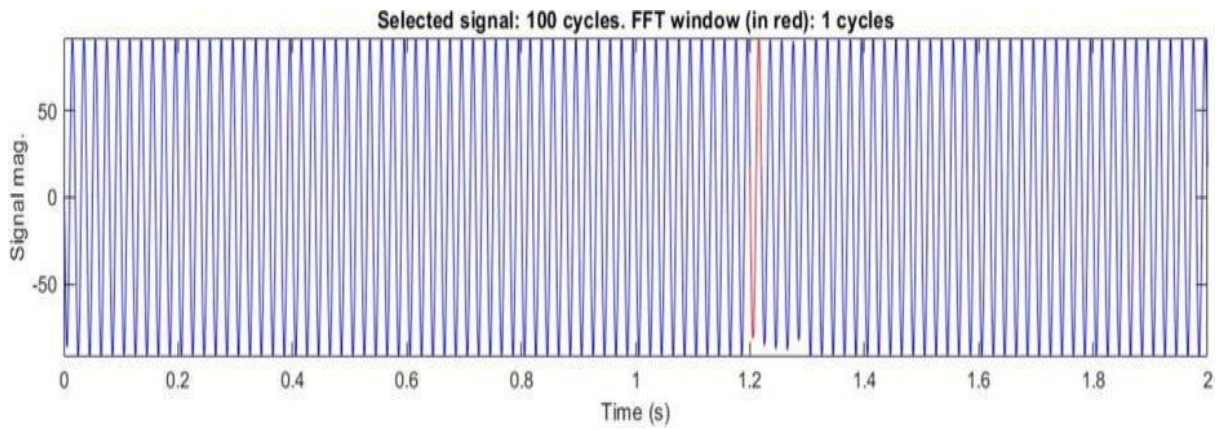
(a)



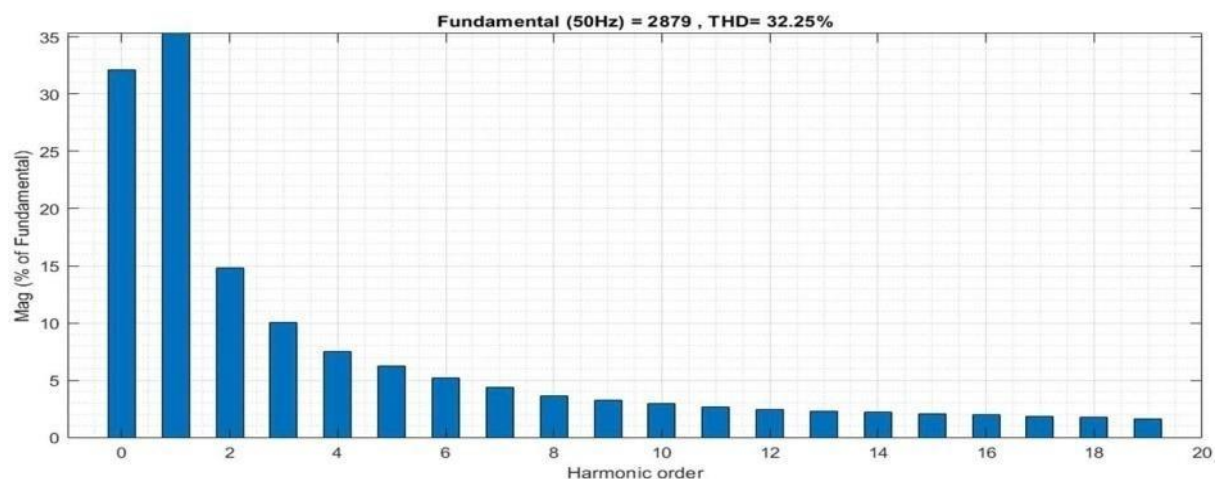
(b)

Fig. 7.13 (a) Load Phase-to-Phase Voltage Signal, (b) FFT Plot of Load Phase-to-Phase Voltage Under Faulty Condition

The signal window and FFT plot for the generator side and load side phase currents are displayed in Figure 7.12 (a) and (b), respectively. As shown in Figs. 7.13 (a) and (b), the FFT window is obtained for one cycle of the signal during the fault that occurs at time  $t=1.2$  seconds.



(a)



(b)

Fig. 7.14 (a) Generation Side Phase Current Signal, (b) FFT Plot of Generation Side Phase Current Under Faulty Condition

According to Fig. 7.14 (b), the total harmonic distortion (THD) for the generator side's phase current during the fault is 32.25%, which is far greater than the IEEE specifications. There is also a noticeable increase in the third and fifth harmonics.

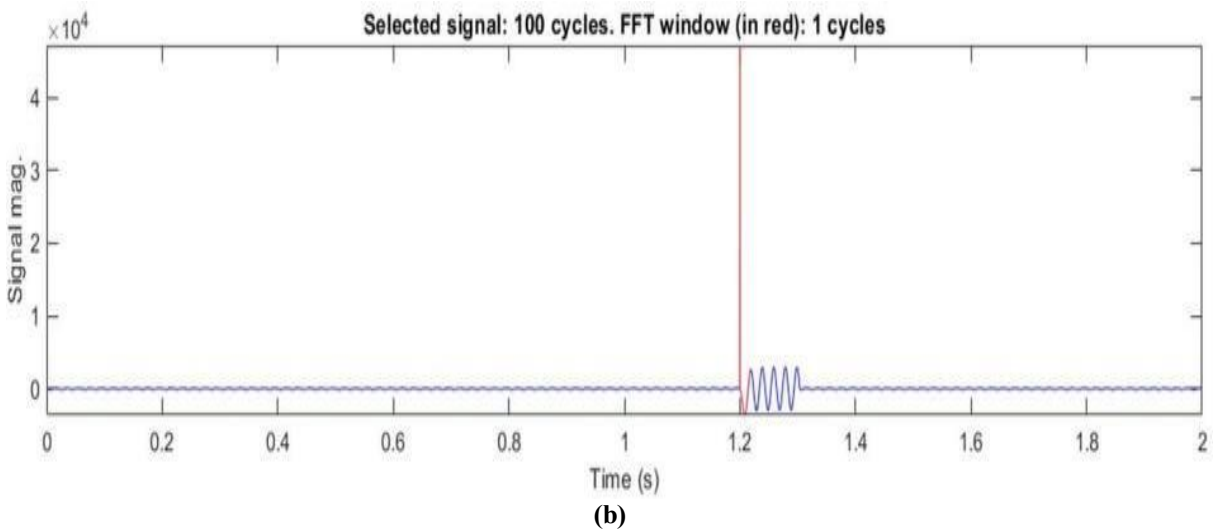
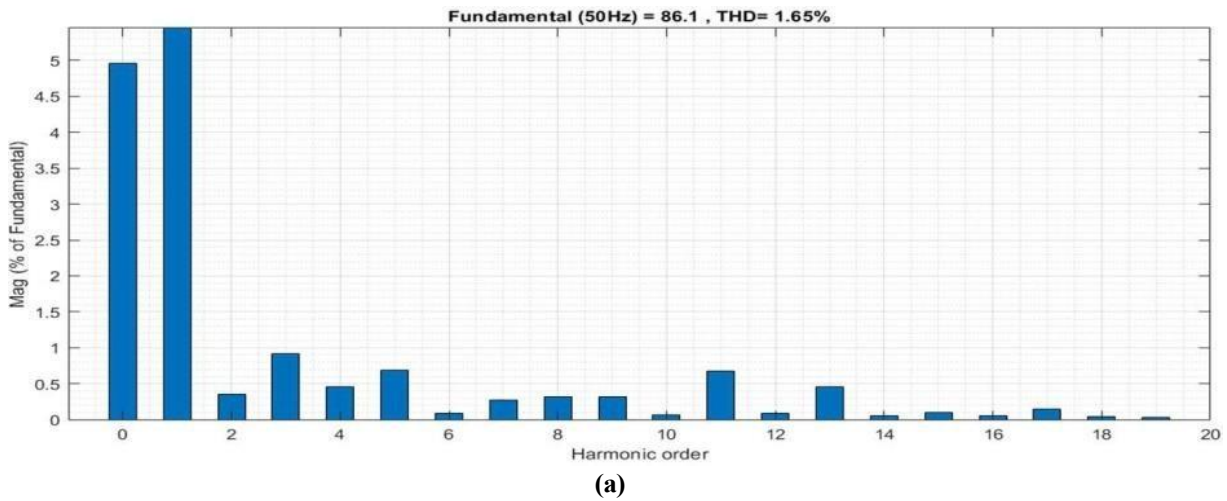


**Fig. 7.15 (a) Load Phase Current Signal, (b) FFT Plot of Load Phase Current Under Faulty Condition**

According to IEEE standards, the phase current of the load during the fault has a total harmonic distortion (THD) of 1.65% at an amplitude of 86.1 A, which is within an acceptable range (Fig. 7.15 (b)). In addition, the load phase current has lower third and fifth harmonics than the generator side.

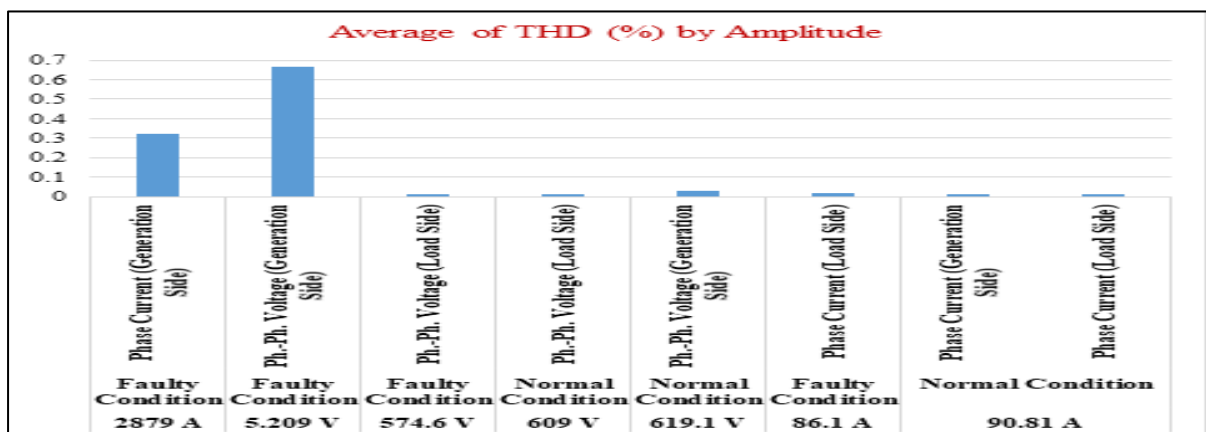


**Fig. 7.16 FFT Analysis**

THD values for  $V_{pp}$  and  $I_{ph}$  on the generating side and load side, both during faults and under normal operating circumstances, are shown in Fig. 7.16. When these THD values are compared, it becomes clear that the system using an ANN-based DVR is more stable and efficient.

**Table-7.1 Comparative Table of DVR Performance During Fault Conditions**

Parameter	Conventional DVR	ANN-Based DVR	Improvement/Impact
Voltage Stability (Load Side)	Distorted (430V)	Stable (440V)	Enhanced voltage stability
Current Stability (Load Side)	Fluctuates (64.23 A)	Stable (65.65 A)	Improved current stability
Voltage THD (Normal)	-	1.20%	IEEE standard compliant
Current THD (Normal)	-	1.18%	IEEE standard compliant
Voltage THD (Fault)	66.36% (Generation)	1.52% (Load)	Lower harmonics on load side
Current THD (Fault)	32.25% (Generation)	1.65% (Load)	Lower harmonics on load side

Compared to the traditional DVR, the ANN-based DVR offers significant advantages, particularly in fault situations. It efficiently lowers THD, maintains steady RMS voltage and current on the load side, and complies with IEEE requirements. These results show how reliable and appropriate the ANN-based DVR is for improving power quality in situations that are prone to faults.

## CONCLUSION

The study presents an artificial neural network (ANN)-based control strategy that demonstrates superior voltage regulation compared to traditional methods, maintaining the DC bus voltage within  $\pm 3.01V$ —well within the IEEE Standard 141-1993 limit of  $\pm 5\%$ . The proposed maximum power point (MPP) tracking methods effectively extract optimal power from renewable sources such as solar and wind. Utilizing the ANN-based control approach, the generator-side voltage is efficiently managed, and the DC bus voltage remains stable. The application of ANN in operating dynamic voltage restorers (DVRs) has proven effective in enhancing power quality, outperforming traditional systems in mitigating voltage sags and swells. The study thoroughly details the problem definition, conceptual framework, proposed control structure, and ANN training methodology. Simulation results confirm the DVR's improved performance under various voltage disturbances. Furthermore, a comparative analysis with the conventional proportional-integral (PI) controller highlights the ANN controller's superior ability to restore voltage while minimizing total harmonic distortion (THD). Simulations also indicate that both standalone and hybrid renewable systems, when controlled via the proposed ANN approach, successfully meet load demands and maintain voltage stability under symmetrical and asymmetrical conditions. Additionally, power transfer from generation to load is effectively and autonomously managed by the ANN-based controller, confirming the robustness and practicality of the proposed method.

## REFERENCES

- [1] Imran Shafi; Harris Khan; Muhammad Siddique Farooq; Isabel de la Torre Diez; Yini Miró; Juan Castanedo Galán and Imran Ashraf 2023. "An Artificial Neural Network-Based Approach for Real-Time Hybrid Wind–Solar Resource Assessment and Power Estimation" *Energies*, Vol.16, issues no. 10, 2023.
- [2] Shafi, I., Mehmood, A., Hafeez, A., Yousaf, M. S., & Khan, M. M. "An artificial neural network-based approach for real-time hybrid wind-solar resource forecasting," *Energies*, vol. 16, no. 10, p. 4171, 2023.
- [3] Sahoo, S., Sahoo, A., & Nayak, J. "Artificial deep neural network in hybrid PV system for controlling the DC link voltage," *International Journal of Photoenergy*, vol. 2022, Article ID 9353470, 2022.
- [4] Aghmadi, A., Hussein, H., & Mohammed, O. "Enhancing energy management system for a hybrid wind-solar-battery based standalone microgrid," *Batteries*, vol. 10, no. 9, p. 297, 2024.
- [5] Kumar, P. S. S., Suresh, P., & Lenine, D. "Performance improvement of integrated microgrid based predictive control scheme," *Advances in Computer Science Research*, vol. 112, pp. 43–50, 2024.
- [6] Roy, P., He, J., Zhao, T. and Singh, Y.V., "Recent advances of wind-solar hybrid renewable energy systems

- for power generation: A review". IEEE Open Journal of the Industrial Electronics Society, Vol. 3, pp. 81-104, 2022.
- [7] Bansal, A.K., "Sizing and forecasting techniques in photovoltaic-wind based hybrid renewable energy system: A review". Journal of Cleaner Production, Vol. 369, pp. 133376-133387, 2022.
- [8] Thirunavukkarasu, M., Sawle, Y. and Lala, H., "A comprehensive review on optimization of hybrid renewable energy systems using various optimization techniques". Renewable and Sustainable Energy Reviews, Vol. 176, pp. 113192-113199, 2023.
- [9] Alexander, A. and Thathan, M. 2015. Modelling and analysis of modular multilevel converter for solar photovoltaic applications to improve power quality. IET Renewable Power Generation 9: 78-88.
- [10] Cholamuthu, P., Irusappan, B., Paramasivam, S.K., Ramu, S.K., Muthusamy, S., Panchal, H., Nuvvula, R.S., Kumar, P.P. and Khan, B., "A grid-connected solar PV/wind turbine based hybrid energy system using ANFIS controller for hybrid series active power filter to improve the power quality". International Transactions on Electrical Energy Systems, Vol. 66, pp. 1425-1445, 2022.
- [11] Abdelkader, A.B., Mouloudi, Y. and Soumeur, M.A., "Integration of renewable energy sources in the dynamic voltage restorer for improving power quality using ANFIS controller". Journal of King Saud University-Engineering Sciences, Vol. 35, pp. 539-548, 2023.
- [12] Goud, B.S., Rekha, R., Jyostna, M.R.L., Sarala, S., Rao, B.L. and Reddy, C.R., "Energy management and power quality improvement in HRES grid-connected system". IEEE International Conference on Electrical Engineering, September 2020, pp. 174-178.
- [13] Ranjan, A. and Choudhary, J., "Enhancement of power quality in grid-connected HRES using UPQC with self-improved Particle Swarm Optimizer in IEEE 14 bus system". Engineering Research Express, Vol. 5, pp. 045018-045029, 2023.
- [14] Cai, W., Li, C., Agbossou, K., Bénard, P. and Xiao, J., "A review of hydrogen-based hybrid renewable energy systems: Simulation and optimization with artificial intelligence". In Journal of Physics: Conference Series, pp. 012012, 2022.
- [15] Kahwash, F., Barakat, B. and Maheri, A., "Coupled thermo-electrical dispatch strategy with AI forecasting for optimal sizing of grid-connected hybrid renewable energy systems". Energy Conversion and Management, Vol. 293, pp. 117460-117471, 2023.
- [16] Maghami, M.R. and Mutambara, A.G.O., "Challenges associated with Hybrid Energy Systems: An artificial intelligence solution". Energy Reports, Vol. 9, pp. 924-940, 2023.
- [17] Godwin Immanuel, D., Suresh Kumar, R., Nagabhooshanam, N., Inkollu, S.R., Salunkhe, S.S., Kamesh, V.V. and Srihari, T., "Grid-Connected RES Integration for Power Optimization Using Multi-Level Inverters and AI Techniques". Electric Power Components and Systems, Vol. 9, pp. 1-17, 2023.
- [18] Uddin, S.M. and Bakar, M.I.A., "Intelligent Voltage Sag Compensation Using an Artificial Neural Network (ANN)-Based Dynamic Voltage Restorer in MATLAB Simulink". International Journal of Integrated Engineering, Vol. 15, pp. 249-261, 2023
- [19] Satyajeeet Sahoo et al. 2022. "Artificial Deep Neural Network in Hybrid PV System for Controlling the Power Management" Hindawi International Journal of Photoenergy, Vol.10, issues no. 02, 2022.
- [20] Ahmed Aghmadi; Hossam Hussein; Osama A. Mohammed 2023. "Enhancing Energy Management System for a Hybrid Wind Solar Battery Based Standalone Microgrid" IEEE International Conference on Environment and Electrical Engineering held during 06-09 June 2023, pp. 1-6.
- [21] P. Sai Sampath Kumar et al. 2023. "Energy Management System for Small Scale Hybrid Wind Solar Battery Based Microgrid" 4th International Conference on Design and Manufacturing Aspects for Sustainable Energy (ICMED-ICMPC 2023).
- [22] Arul, P.G., Ramachandramurthy, V.K. and Rajkumar, R. K., "Control strategies for a hybrid renewable energy system: A Review," Renewable and Sustainable Energy Reviews, vol. 42, pp. 597-608, 2015.
- [23] Lazarov, V., Notton, G., Zarkov, Z. and Bochev, I. "Hybrid power systems with renewable energy sources types, structures, trends for research and development," In: Proceedings of 11th International conference on electrical machines, drives and power systems, held at Bulgaria during September 15-16, 2005, pp.515-520.
- [24] Siddaiah, R. and Saini, R.P., "A review on planning, configurations, modeling and optimization techniques of hybrid renewable energy systems for off grid applications," Renewable and Sustainable Energy Reviews vol. 58, pp. 376-396, 2016.
- [25] Chauhan, A. and Saini, R.P., "A review on Integrated Renewable Energy System based power generation for stand-alone applications: Configurations, storage options, sizing methodologies and control," Renewable and Sustainable Energy Reviews vol. 38, pp. 99-120, 2014.
- [26] Nehrir, M. H., Wang, C., Strunz, H. Aki, Ramakumar, R., Bing, J., Miao, Z. and Salameh, "A review of hybrid renewable/alternative energy systems for electric power generation: configurations, control, and applications," IEEE Transactions on Sustainable Energy vol. 2, no.1, pp. 392-403, 2011.
- [27] Wang, C. and Nehrir, M. H., "Power management of a stand-alone wind/photovoltaic/ fuel cell energy system," IEEE Transactions on energy conversion vol. 23, no. 5, pp. 957-967, 2008.

- [28] M. Aarif; D. Joshi; R. Jangid and S.S. Sharma, "Grid Power Smoothing Management for Direct Drive PMSG Variable Speed Wind Energy Conversion System with Multilevel Converter", IEEE 7th International Conference on ICT for Sustainable Development, Organized by Global Knowledge Foundation during 29-30, July 2022 at Goa, India.
- [29] Y. Joshi; J.k Maherchandani; V.K Yadav; R. Jangid; S. Vyas and S.S Sharma, "Performance Improvement of Standalone Battery Integrated Hybrid System" IEEE 7th International Conference on Electrical Energy Systems (ICEES), Organized by Sri Sivasubramaniya Nadar College of Engineering during 11-13 Feb. 2021 at Chennai, India.
- [30] R. Jangid; J.k Maherchandani; R.R. Joshi and B.D Vairagi, "Development of Advance Energy Management Strategy for Standalone Hybrid Wind & PV System Considering Rural Application", IEEE 2nd International Conference on Smart Systems and Inventive Technology, Organized by Francis Xavier Engineering College during November 27-29, 2019 at Tirunelveli, India.
- [31] R. Jangid; K. Parikh and P. Anjana, "Reducing the Voltage Sag and Swell Problem in Distribution System Using Dynamic Voltage Restorer with PI Controller", International Journal of Soft Computing and Engineering, ISSN: 2231-2307, Vol.-3, Issue-6, January 2014.
- [32] R. Jangid; J.k Maherchandani; V.K Yadav and R.K Swami, "Energy Management of Standalone Hybrid Wind-PV System", Journal of Intelligent Renewable Energy Systems (John Wiley & Sons, Inc.) Pages 179-198, 2022.
- [33] H. Kumawat and R. Jangid, "Using AI Techniques to Improve the Power Quality of Standalone Hybrid Renewable Energy Systems", Crafting a Sustainable Future Through Education and Sustainable Development, IGI Global, Pages 219-228, 2023.
- [34] H. Kumawat; R. Jangid, "Performance and Investigation of Two Drive Train Interfaced Permanent Magnet Synchronous Generator for Wind Energy Conversion System", Journal of Emerging Technologies and Innovative Research, ISSN:2349-5162, Volume 7, Issue 1, January 2020.
- [35] R. Jangid et. al., "Smart Household Demand Response Scheduling with Renewable Energy Resources", IEEE Third International Conference on Intelligent Computing and Control System, Organized by Vaigai College of Engineering during May 15-17, 2019 at Madurai, India.
- [36] S. Kumar; R. Jangid and K. Parikh "Comparative Performance Analysis of Adaptive Neuro-Fuzzy Inference System (ANFIS) & ANN Algorithms Based MPPT Energy Harvesting in Solar PV System." International Journal of Technical Research and Science, vol. 8, Issue 3, March 2023.
- [37] S. Sharma; R. Jangid and K. Parikh "Development of Intelligent Control Strategy for Power Quality Improvement of Hybrid RES Using AI Technique" International Journal of Technical Research and Science, vol. VIII, Issue II, Feb. 2023.
- [38] L. Jhala et al., "Development of Control Strategy for Power Management in Hybrid Renewable Energy System" International Journal of Technical Research and Science, vol. VI, Issue XII, Dec. 2021.
- [39] Mohod, S.W. and Aware, M.V., "A STATCOM-control scheme for grid connected wind energy system for power quality improvement," IEEE Systems Journal vol. 4, no. 2, pp. 346-352, 2010.
- [40] Frangieh, W. and Najjar, M. B., "Active control for power quality improvement in hybrid power systems," In: Proceedings of IEEE 3rd International Conference on Technological Advances in Electrical, Electronics and Computer Engineering held at Lebanon during April 29-30, 2015, pp. 218-223.
- [41] Rini, T. H. and Razzak, M. A., "Voltage and power regulation in a solar-wind hybrid energy system," In: Proceedings of IEEE International WIE Conference on Electrical and Computer held at Dhaka during December 19-20, 2015, pp. 231-234.
- [42] Prasad, V., "Voltage Compensation in a grid connected hybrid system using dynamic voltage restorer". In: Proceedings of IEEE International Conference on Power Instrumentation Control and Computing held at Thrissur during December 9-11, 2015, pp. 1-5.
- [43] Jayasankar, V. N. and Vinatha, U., "Implementation of adaptive fuzzy controller in a grid connected wind-solar hybrid energy system with power quality improvement features," In: Proceedings of IEEE Biennial International Conference on Power and Energy Systems: Towards Sustainable Energy held at Bengaluru during January 21-23, 2016, pp. 1-5.